AIAA JOURNAL
Vol. 48, No. 12, December 2010

Technical Notes

Stability of Gliding Flight of a Swallowtail Butterfly

Makoto Okamoto,* Shigeru Sunada,† and Hiroshi Tokutake‡
Osaka Prefecture University, Osaka 599-8531, Japan

DOI: 10.2514/1.43078

Nomenclature

a_D	=	coefficient of α^2 for C_D
b_W	=	wing length × 2
c	=	chord length at y_W
$\bar{c}$	=	mean aerodynamic chord
C_D	=	drag coefficient of a wing element
C_L	=	lift coefficient of a wing element
C_{L0}	=	lift coefficient when α_W is zero
$C_{L0,\Lambda=0}$	=	C_{L0} when Λ is zero
C_M	=	pitching moment coefficient of a wing element
$C_{D\alpha}$	=	$\partial C_D/\partial\alpha_W$
C_{D0}	=	drag coefficient when α_W is zero
$\bar{C}_{D0}$, $\bar{C}_{D\alpha}$	=	C_{D0} and $C_{D\alpha}$ of swallowtail
$\mathrm{d}D$	=	drag acting on a wing element
$\mathrm{d}F_{xW}$, $\mathrm{d}F_{yW}$, $\mathrm{d}F_{zW}$	=	forces acting on a wing element in x_W, y_W, and z_W directions
$\mathrm{d}L$	=	lift acting on a wing element
$\mathrm{d}M$	=	pitching moment acting on a wing element
$\mathrm{d}M_{xW}$, $\mathrm{d}M_{yW}$, $\mathrm{d}M_{zW}$	=	moments acting on a wing element about x_W, y_W, and z_W axes
F_{xS}, F_{yS}, F_{zS}	=	forces acting on a right wing in x_S, y_S, and z_S directions
$F_{xS,L}$, $F_{zS,L}$	=	forces acting on a load cell in x_S and z_S directions
g	=	acceleration of gravity
h	=	distance between centers of gravity and a load cell
I_{xxS}, I_{yyS}, I_{zzS}	=	moments of inertia about x_S, y_S, and z_S axes
L'_β, L'_p, L'_r, N'_β, N'_p, N'_r	=	primed derivatives
M_{xS}, M_{yS}, M_{zS}	=	moments acting on a right wing about x_S, y_S, and z_S axes
$M_{yS,L}$	=	moment acting on a load cell about y_S axis
m_{xS}, m_{yS}, m_{zS}	=	total of a swallowtail's mass and added masses of wings in x_S, y_S, and z_S directions
p, q, r	=	angular velocities of a swallowtail about x_S, y_S, and z_S axes
Re	=	Reynolds number
S	=	wing area
S_W	=	area of upper (or lower) surface of wings
u, v, w	=	disturbance of velocities of a swallowtail in x_S, y_S, and z_S directions
U_S, V_S, W_S	=	velocities of a wing element at y_W in x_S, y_S, and z_S directions
U_W, V_W, W_W	=	velocities of a wing element at y_W in x_W, y_W, and z_W directions
U_0	=	forward velocity of a gliding swallowtail
X_u, X_α, X_q, Z_u, Z_α, Z_q, M_u, M_α, M_q	=	stability derivatives for longitudinal motion
x_B, y_B, z_B	=	body coordinate system
x_S, y_S, z_S	=	stability coordinate system
x_W, y_W, z_W	=	wing fixed coordinate system
Y_β, Y_p, Y_r, L_β, L_p, L_r, N_β, N_p, N_r	=	stability derivatives for lateral-directional motion
α	=	angle of attack
α_W	=	angle of attack of a wing element at y_W
α_0	=	angle of attack of a gliding swallowtail
β	=	sideslip angle
Γ	=	dihedral angle
Δm_{xS}, Δm_{zS}	=	added masses of wings in x_S and z_S directions
θ_0	=	pitch angle
Λ	=	sweepback angle
λ	=	eigenvalue
ρ	=	density of air
φ	=	roll angle
σ	=	real part of an eigenvalue
σ_S, σ_R, σ_D, σ_{LP}, σ_{SP}	=	real part of an eigenvalue for spiral, roll, Dutch roll, long-period, and short-period modes
ω	=	imaginary part of an eigenvalue
ω_D, ω_{LP}, ω_{SP}	=	imaginary parts of an eigenvalue for Dutch roll, long-period, and short-period modes

Received 5 January 2009; revision received 3 October 2009; accepted for publication 16 August 2010.

*Graduate Student, Department of Aerospace Engineering, 1-1, Gakuenmachi, Nakaku, Sakai.

†Associate Professor, Department of Aerospace Engineering, 1-1, Gakuenmachi, Nakaku, Sakai; sunada@aero.osakafu-u.ac.jp. Member AIAA.

‡Assistant Professor, Department of Aerospace Engineering, 1-1, Gakuenmachi, Nakaku, Sakai. Member AIAA.

Introduction

OKAMOTO et al. [1] recently analyzed the flight stability of the lateral-directional motion of a swallowtail butterfly *Pupilio xuthus*. Their analysis showed that a swallowtail glides with a high dihedral angle due to the stability of the spiral mode and that the relation between a dihedral angle and the stability of the Dutch roll mode is strongly affected by *Re*. In the present analysis, the flight stability of the longitudinal motion of the same swallowtail is analyzed to investigate the stability of the longitudinal motion at a high dihedral angle. Furthermore, the flight stability of the lateral-directional motion of the same swallowtail will be analyzed again. A main improvement from the previous analysis is the measurement of the pitching moment with high accuracy. The effects of *Re* on all the modes of the longitudinal and the lateral-directional motions will be investigated.

Methods

The detailed analytical method is stated in [1]. The following are the differences between the present and previous analyses:

1) In the present analysis, the added mass, not only in the y_S axis but also in x_S and z_S, was considered as follows:

$$\Delta m_{xS} = 2\rho\pi \int_0^{b_W/2} \left(\frac{c}{2}\right)^2 \mathrm{d}y_W \cos\Gamma \sin\alpha_0$$

$$\Delta m_{zS} = 2\rho\pi \int_0^{b_W/2} \left(\frac{c}{2}\right)^2 \mathrm{d}y_W \cos\Gamma \cos\alpha_0 \quad (1)$$

2) In both the present and previous analyses, to obtain C_L, $\partial C_L/\partial\alpha_W$, C_D, $\partial C_D/\partial\alpha_W$, C_M, and $\partial C_M/\partial\alpha_W$, wind-tunnel tests were performed using a model wing. As shown in Fig. 1, the installation of the model wing on the load cell was revised. The pitching moment around the center of gravity was measured more precisely than in the previous analysis. The load cell (MMS-2402, Nissho Corporation) measured $F_{xS,L}$, $F_{zS,L}$, and $M_{yS,L}$. The forces and the moment acting at the center of gravity of the swallowtail were obtained from the measured $F_{xS,L}$, $F_{zS,L}$, and $M_{yS,L}$ by

$$F_{xS} = F_{xS,L}, \qquad F_{zS} = F_{zS,L}, \qquad M_{yS} = M_{yS,L} + F_{xS,L}h \tag{2}$$

Here, the forces and the moments acting on the cylinder connecting the wings and the load cell were considered negligible and therefore ignored. The parameters of the measurements were $\Gamma = 10, 20, 30,$ and $45°$, and $\alpha_0 = 0, 2, 4, \ldots, 30°$. The newly obtained C_L, C_D, and C_M are shown in Fig. 2. C_M was determined as follows. First, the averaged 25% chordwise position is defined as

$$\bar{x}_W = \frac{2}{S_W}\int_0^{b_W/2} x_W c\,\mathrm{d}y_W, \qquad \bar{y}_W = \frac{2}{S_W}\int_0^{b_W/2} y_W c\,\mathrm{d}y_W \tag{3}$$

The x_S and z_S coordinates of this point are given by

$$\begin{bmatrix}\bar{x}_S\\ \bar{z}_S\end{bmatrix} = \begin{bmatrix}1 & -\alpha_W\cos\Gamma\\ -\alpha_W & -\sin\Gamma\end{bmatrix}\begin{bmatrix}\bar{x}_W\\ \bar{y}_W\end{bmatrix} \tag{4}$$

The moment coefficient C_M corresponds to a nondimensional moment around the axis, which is through the averaged 25% chordwise position and parallel to the y_W axis. C_M is given by

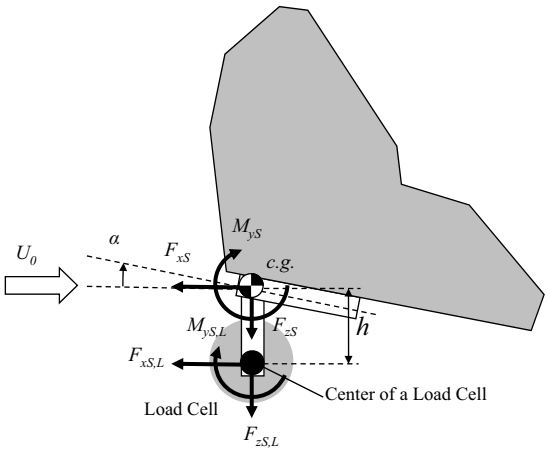

a)

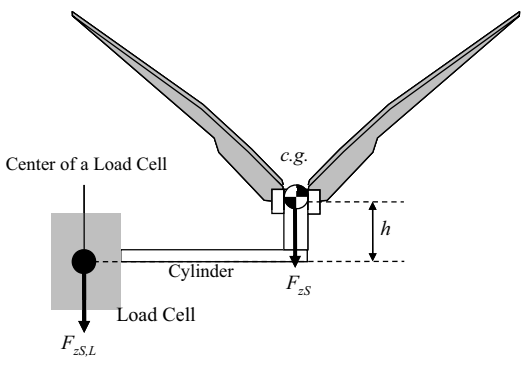

b)

Fig. 1 Model wing used in wind-tunnel tests to measure lift, drag, and coefficients of model wing: a) front and b) side.

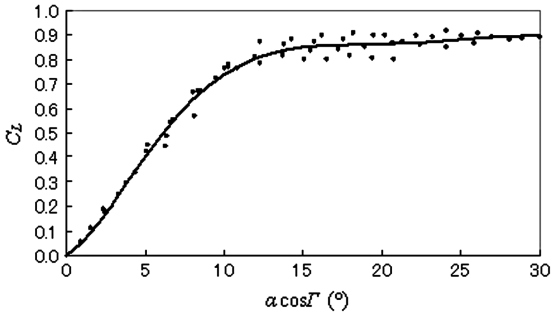

a)

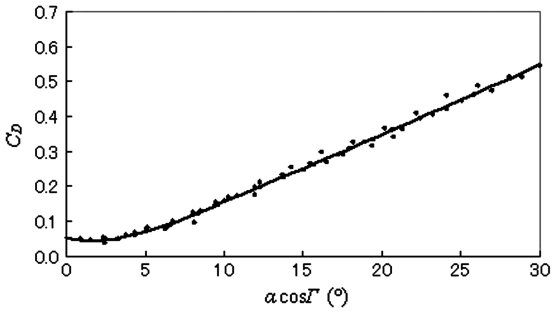

b)

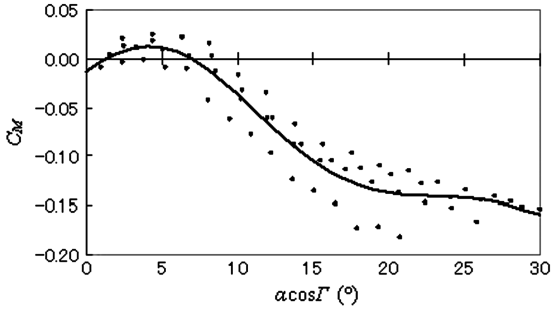

c)

Fig. 2 Experimentally obtained wing characteristics of a model wing: a) lift coefficients C_L, b) drag coefficients C_D, and c) moment coefficient C_M.

$$C_M = \frac{2}{\rho U_0^2 S_W \bar{c}}\frac{(M_{yS} - F_{xS}\bar{z}_S + F_{zS}\bar{x}_S)}{\cos\Gamma} = \frac{2(M_{yS} - F_{xS}\bar{z}_S + F_{zS}\bar{x}_S)}{\rho U_0^2 S\bar{c}}$$

3) The more precise pitching moment enabled stricter application of the trimmed condition concerning pitching moment $M_{yS}(\alpha_0\cos\Gamma) = 0$. Note that the pitching moments around the center of gravity were approximately zero for all angles of attack and the dihedral angles in the previous analysis.

Obtaining the expressions for the stability derivatives by blade element theory is summarized as follows. The stability derivatives due to both the right and left wings are

$$\begin{bmatrix}X_*\\ Z_*\\ M_*\end{bmatrix} = 2\begin{bmatrix}\frac{1}{m_{xS}}\frac{\partial F_{xS}}{\partial *}\\ \frac{1}{m_{zS}}\frac{\partial F_{zS}}{\partial *}\\ \frac{1}{I_{yyS}}\frac{\partial M_{yS}}{\partial *}\end{bmatrix} \quad (* = u, \alpha, q)$$

$$\begin{bmatrix}Y_*\\ L_*\\ N_*\end{bmatrix} = 2\begin{bmatrix}\frac{1}{m_{yS}}\frac{\partial F_{yS}}{\partial *}\\ \frac{1}{I_{xxS}}\frac{\partial M_{xS}}{\partial *}\\ \frac{1}{I_{zzS}}\frac{\partial M_{zS}}{\partial *}\end{bmatrix}, \quad (* = \beta, p, r) \tag{5}$$

Here, F_{xS}, F_{yS}, F_{zS}, M_{xS}, M_{yS}, and M_{zS} are the forces and moments acting only on the right wings. The stability derivatives in the stability coordinate system due to the right wings are given by

$$\frac{\partial}{\partial^*}\begin{bmatrix} F_{xS} & M_{xS} \\ F_{yS} & M_{yS} \\ F_{zS} & M_{zS} \end{bmatrix} = \begin{bmatrix} 1 & -\alpha_0 \sin\Gamma & \alpha_0 \cos\Gamma \\ 0 & \cos\Gamma & \sin\Gamma \\ -\alpha_0 & -\sin\Gamma & \cos\Gamma \end{bmatrix} \times \int_0^{b_W/2} \frac{\partial}{\partial^*}\begin{bmatrix} \mathrm{d}F_{xW} & \mathrm{d}M_{xW} \\ \mathrm{d}F_{yW} & \mathrm{d}M_{yW} \\ \mathrm{d}F_{zW} & \mathrm{d}M_{zW} \end{bmatrix} \tag{6}$$

The stability derivative due to the right wings is obtained as follows. The forces and moments acting on a wing element on the right wings, $\mathrm{d}F_{xW}$, $\mathrm{d}F_{yW}$, $\mathrm{d}F_{zW}$, $\mathrm{d}M_{xW}$, and $\mathrm{d}M_{zW}$, are expressed by

$$\begin{bmatrix} \mathrm{d}F_{xW} \\ \mathrm{d}F_{yW} \\ \mathrm{d}F_{zW} \end{bmatrix} = \begin{bmatrix} \alpha_W & -1 \\ 0 & 0 \\ -1 & -\alpha_W \end{bmatrix} \begin{bmatrix} \mathrm{d}L(\alpha_W, \beta_W, U^2) \\ \mathrm{d}D(\alpha_W, U^2) \end{bmatrix}$$

$$\begin{bmatrix} \mathrm{d}M_{xW} \\ \mathrm{d}M_{yW} \\ \mathrm{d}M_{zW} \end{bmatrix} = \begin{bmatrix} x_W \\ y_W \\ 0 \end{bmatrix} \times \begin{bmatrix} \mathrm{d}F_{xW} \\ \mathrm{d}F_{yW} \\ \mathrm{d}F_{zW} \end{bmatrix} + \begin{bmatrix} 0 \\ \mathrm{d}M(\alpha_W, U^2) \\ 0 \end{bmatrix} \tag{7}$$

where $\alpha_W = W_W/U_W$ and $\beta_W = V_W/U_W$. Coordinate (x_W, y_W) is the 25% chordwise position of the wing element. The pitching moment around the axis is $\mathrm{d}M$, which is parallel to the y_W axis and through the 25% chordwise position of the wing element. Differentiating these equations by $* = (u, \beta, \alpha, p, q, r)$, the following equations are obtained:

$$\frac{\partial}{\partial^*}\begin{bmatrix} \mathrm{d}F_{xW} \\ \mathrm{d}F_{yW} \\ \mathrm{d}F_{zW} \end{bmatrix} = \begin{bmatrix} \frac{\partial \alpha_W}{\partial^*}\mathrm{d}L \\ 0 \\ -\frac{\partial \alpha_W}{\partial^*}\mathrm{d}D \end{bmatrix} + \begin{bmatrix} \alpha_W & -1 \\ 0 & 0 \\ -1 & -\alpha_W \end{bmatrix} \begin{bmatrix} \frac{\partial \mathrm{d}L}{\partial \alpha_W}\frac{\partial \alpha_W}{\partial^*} + \frac{\partial \mathrm{d}L}{\partial \beta_W}\frac{\partial \beta_W}{\partial^*} + \frac{\partial \mathrm{d}L}{\partial U^2}\frac{\partial U^2}{\partial^*} \\ \frac{\partial \mathrm{d}D}{\partial \alpha_W}\frac{\partial \alpha_W}{\partial^*} + \frac{\partial \mathrm{d}D}{\partial U^2}\frac{\partial U^2}{\partial^*} \end{bmatrix}$$

$$= \begin{bmatrix} \mathrm{d}L + \alpha_W \frac{\partial \mathrm{d}L}{\partial \alpha_W} - \frac{\partial \mathrm{d}D}{\partial \alpha_W} & \alpha_W \frac{\partial \mathrm{d}L}{\partial \beta_W} & \alpha_W \frac{\partial \mathrm{d}L}{\partial U^2} - \frac{\partial \mathrm{d}D}{\partial U^2} \\ 0 & 0 & 0 \\ -\mathrm{d}D - \frac{\partial \mathrm{d}L}{\partial \alpha_W} - \alpha_W \frac{\partial \mathrm{d}D}{\partial \alpha_W} & -\frac{\partial \mathrm{d}L}{\partial \beta_W} & -\frac{\partial \mathrm{d}L}{\partial U^2} - \alpha_W \frac{\partial \mathrm{d}D}{\partial U^2} \end{bmatrix} \begin{bmatrix} \frac{\partial \alpha_W}{\partial^*} \\ \frac{\partial \beta_W}{\partial^*} \\ \frac{\partial U^2}{\partial^*} \end{bmatrix} \tag{8}$$

$$\frac{\partial}{\partial^*}\begin{bmatrix} \mathrm{d}M_{xW} \\ \mathrm{d}M_{yW} \\ \mathrm{d}M_{zW} \end{bmatrix} = \begin{bmatrix} x_W \\ y_W \\ 0 \end{bmatrix} \times \frac{\partial}{\partial^*}\begin{bmatrix} \mathrm{d}F_{xW} \\ \mathrm{d}F_{yW} \\ \mathrm{d}F_{zW} \end{bmatrix} + \begin{bmatrix} 0 \\ \frac{\partial \mathrm{d}M}{\partial \alpha_W}\frac{\partial \alpha_W}{\partial^*} + \frac{\partial \mathrm{d}M}{\partial U^2}\frac{\partial U^2}{\partial^*} \\ 0 \end{bmatrix}$$

$$= \begin{bmatrix} y_W \frac{\partial \mathrm{d}F_{zW}}{\partial^*} \\ -x_W \frac{\partial \mathrm{d}F_{xW}}{\partial^*} \\ -y_W \frac{\partial \mathrm{d}F_{xW}}{\partial^*} \end{bmatrix} + \begin{bmatrix} 0 & 0 & 0 \\ \frac{\partial \mathrm{d}M}{\partial \alpha_W} & 0 & \frac{\partial \mathrm{d}M}{\partial U^2} \\ 0 & 0 & 0 \end{bmatrix} \begin{bmatrix} \frac{\partial \alpha_W}{\partial^*} \\ \frac{\partial \beta_W}{\partial^*} \\ \frac{\partial U^2}{\partial^*} \end{bmatrix} \tag{9}$$

In the previous equations, $\partial \alpha_W/\partial^*$, $\partial \beta_W/\partial^*$, and $\partial U^2/\partial^*$ $(* = u, \beta, \alpha, p, q, r)$ are obtained as follows:

$$* = u: \begin{bmatrix} U_S \\ V_S \\ W_S \end{bmatrix} = \begin{bmatrix} U_0 + u \\ 0 \\ 0 \end{bmatrix}$$

Then,

$$\begin{bmatrix} U_W \\ V_W \\ W_W \end{bmatrix} = \begin{bmatrix} U_0 + u \\ -(U_0 + u)\alpha_0 \sin\Gamma \\ (U_0 + u)\alpha_0 \cos\Gamma \end{bmatrix}$$

$$\begin{bmatrix} \alpha_W \\ \beta_W \\ U^2 \end{bmatrix} = \begin{bmatrix} \alpha_0 \cos\Gamma \\ -\alpha_0 \sin\Gamma \\ U_0^2 + 2U_0 u \end{bmatrix}$$

Therefore,

$$\frac{\partial \alpha_W}{\partial u} = 0, \qquad \frac{\partial \beta_W}{\partial u} = 0, \qquad \frac{\partial U^2}{\partial u} = 2U_0 \tag{10a}$$

$$* = \beta: \begin{bmatrix} U_S \\ V_S \\ W_S \end{bmatrix} = \begin{bmatrix} U_0 \\ \beta U_0 \\ 0 \end{bmatrix}$$

Then,

$$\begin{bmatrix} U_W \\ V_W \\ W_W \end{bmatrix} = \begin{bmatrix} U_0 \\ -U_0\alpha_0 \sin\Gamma + \beta U_0 \cos\Gamma \\ U_0\alpha_0 \cos\Gamma + \beta U_0 \sin\Gamma \end{bmatrix}$$

$$\begin{bmatrix} \alpha_W \\ \beta_W \\ U^2 \end{bmatrix} = \begin{bmatrix} \alpha_0 \cos\Gamma + \beta \sin\Gamma \\ -\alpha_0 \sin\Gamma + \beta \cos\Gamma \\ U_0^2 \end{bmatrix}$$

Therefore,

$$\frac{\partial \alpha_W}{\partial \beta} = \sin\Gamma, \qquad \frac{\partial \beta_W}{\partial \beta} = \cos\Gamma, \qquad \frac{\partial U^2}{\partial \beta} = 0 \tag{10b}$$

$$* = \alpha: \begin{bmatrix} U_S \\ V_S \\ W_S \end{bmatrix} = \begin{bmatrix} U_0 \\ 0 \\ \alpha U_0 \end{bmatrix}$$

Then,

$$\begin{bmatrix} U_W \\ V_W \\ W_W \end{bmatrix} = \begin{bmatrix} U_0 \\ -U_0\alpha_0 \sin\Gamma - \alpha U_0 \sin\Gamma \\ U_0\alpha_0 \cos\Gamma + \alpha U_0 \cos\Gamma \end{bmatrix}$$

$$\begin{bmatrix} \alpha_W \\ \beta_W \\ U^2 \end{bmatrix} = \begin{bmatrix} \alpha_0 \cos\Gamma + \alpha \cos\Gamma \\ -\alpha_0 \sin\Gamma - \alpha \sin\Gamma \\ U_0^2 \end{bmatrix}$$

Therefore,

$$\frac{\partial \alpha_W}{\partial \alpha} = \cos\Gamma, \qquad \frac{\partial \beta_W}{\partial \alpha} = -\sin\Gamma, \qquad \frac{\partial U^2}{\partial \alpha} = 0 \tag{10c}$$

$$* = p: \begin{bmatrix} U_S \\ V_S \\ W_S \end{bmatrix} = \begin{bmatrix} U_0 \\ -pz_S \\ py_S \end{bmatrix}$$

Then,

$$\begin{bmatrix} U_W \\ V_W \\ W_W \end{bmatrix} = \begin{bmatrix} U_0 \\ -U_0\alpha_0 \sin\Gamma - px_W\alpha_0 \cos\Gamma \\ U_0\alpha_0 \cos\Gamma + p(x_W\alpha_0 \sin\Gamma + y_W) \end{bmatrix}$$

$$\begin{bmatrix} \alpha_W \\ \beta_W \\ U^2 \end{bmatrix} = \begin{bmatrix} \alpha_0 \cos\Gamma + \frac{p}{U_0}(x_W\alpha_0 \sin\Gamma + y_W) \\ -\alpha_0 \sin\Gamma - \frac{p}{U_0}x_W\alpha_0 \cos\Gamma \\ U_0^2 \end{bmatrix}$$

Therefore,

$$\frac{\partial \alpha_W}{\partial p} = \frac{1}{U_0}(x_W \alpha_0 \sin\Gamma + y_W), \qquad \frac{\partial \beta_W}{\partial p} = -\frac{1}{U_0} x_W \alpha_0 \cos\Gamma$$

$$\frac{\partial U^2}{\partial \beta} = 0 \tag{10d}$$

$$* = q: \begin{bmatrix} U_S \\ V_S \\ W_S \end{bmatrix} = \begin{bmatrix} U_0 + q z_S \\ 0 \\ -q x_S \end{bmatrix}$$

Then,

$$\begin{bmatrix} U_W \\ V_W \\ W_W \end{bmatrix} = \begin{bmatrix} U_0 - q y_W \sin\Gamma \\ -U_0 \alpha_0 \sin\Gamma + q x_W \sin\Gamma \\ U_0 \alpha_0 \cos\Gamma - q x_W \cos\Gamma \end{bmatrix}$$

$$\begin{bmatrix} \alpha_W \\ \beta_W \\ U^2 \end{bmatrix} \approx \begin{bmatrix} \alpha_0 \cos\Gamma - \frac{q}{U_0} x_W \cos\Gamma \\ -\alpha_0 \sin\Gamma + q x_W \sin\Gamma \\ U_0^2 - 2 U_0 q y_W \sin\Gamma \end{bmatrix}$$

Therefore,

$$\frac{\partial \alpha_W}{\partial q} \approx -\frac{1}{U_0} x_W \cos\Gamma, \qquad \frac{\partial \beta_W}{\partial q} = x_W \sin\Gamma$$

$$\frac{\partial U^2}{\partial q} = -2 U_0 y_W \sin\Gamma \tag{10e}$$

$$* = r: \begin{bmatrix} U_S \\ V_S \\ W_S \end{bmatrix} = \begin{bmatrix} U_0 - r y_S \\ r x_S \\ 0 \end{bmatrix}$$

Then,

$$\begin{bmatrix} U_W \\ V_W \\ W_W \end{bmatrix} = \begin{bmatrix} U_0 - r y_W \cos\Gamma \\ -U_0 \alpha_0 \sin\Gamma + r x_W \cos\Gamma \\ U_0 \alpha_0 \cos\Gamma + r(x_W \sin\Gamma - y_W \alpha_0) \end{bmatrix}$$

$$\begin{bmatrix} \alpha_W \\ \beta_W \\ U^2 \end{bmatrix} \approx \begin{bmatrix} \alpha_0 \cos\Gamma + \frac{r}{U_0}(x_W \sin\Gamma - y_W \alpha_0) \\ -\alpha_0 \sin\Gamma + \frac{r}{U_0} x_W \cos\Gamma \\ U_0^2 - 2 U_0 r y_W \cos\Gamma \end{bmatrix}$$

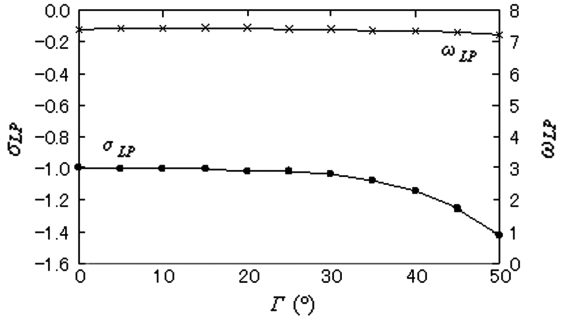

a)

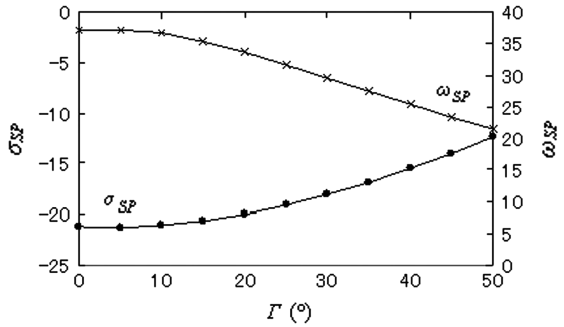

b)

Fig. 3 Eigenvalues of two modes of longitudinal motion: a) long period and b) short period.

Therefore,

$$\frac{\partial \alpha_W}{\partial r} \approx \frac{1}{U_0}(x_W \sin\Gamma - y_W \alpha_0), \qquad \frac{\partial \beta_W}{\partial r} \approx \frac{1}{U_0} x_W \cos\Gamma$$

$$\frac{\partial U^2}{\partial r} = -2 U_0 y_W \cos\Gamma \tag{10f}$$

Considering $\mathrm{d}L = \frac{1}{2}\rho U^2 C_L c \mathrm{d}y_W$, $\mathrm{d}D = \frac{1}{2}\rho U^2 C_D c \mathrm{d}y_W$, and $\mathrm{d}M = \frac{1}{2}\rho U^2 \bar{c} C_M c \mathrm{d}y_W$, the following equations are obtained:

$$\begin{cases} \frac{\partial \mathrm{d}L}{\partial \alpha_W} = \frac{1}{2}\rho U^2 \frac{\partial C_L}{\partial \alpha_W} c \mathrm{d}y_W \\ \frac{\partial \mathrm{d}L}{\partial \beta_W} = \frac{1}{2}\rho U^2 \frac{\partial C_L}{\partial \beta_W} c \mathrm{d}y_W \\ \frac{\partial \mathrm{d}L}{\partial U^2} = \frac{1}{2}\rho C_L c \mathrm{d}y_W \\ \frac{\partial \mathrm{d}D}{\partial \alpha_W} = \frac{1}{2}\rho U^2 \frac{\partial C_D}{\partial \alpha_W} c \mathrm{d}y_W \\ \frac{\partial \mathrm{d}D}{\partial U^2} = \frac{1}{2}\rho C_D c \mathrm{d}y_W \\ \frac{\partial \mathrm{d}M}{\partial \alpha_W} = \frac{1}{2}\rho U^2 \bar{c} \frac{\partial C_M}{\partial \alpha_W} c \mathrm{d}y_W \\ \frac{\partial \mathrm{d}M}{\partial U^2} = \frac{1}{2}\rho \bar{c} C_M c \mathrm{d}y_W \end{cases} \tag{11}$$

Substituting Eqs. (6–11) into Eq. (5) and using the values of C_L, $\partial C_L/\partial \alpha_W$, C_D, $\partial C_D/\partial \alpha_W$, C_M, $\partial C_M/\partial \alpha_W$, and $\partial C_L/\partial \beta_W$, the stability derivatives can be calculated. The values of C_L, $\partial C_L/\partial \alpha_W$, C_D, $\partial C_D/\partial \alpha_W$, C_M, and $\partial C_M/\partial \alpha_W$, which are at $\alpha_W = \alpha_0 \cos\Gamma$, will

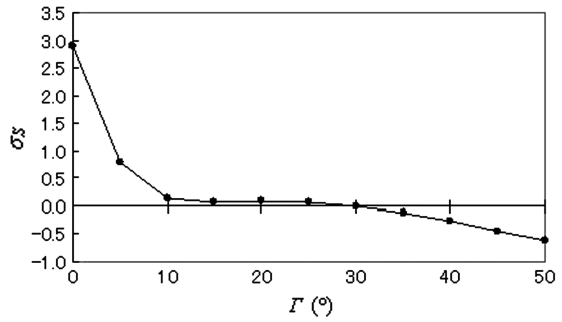

a)

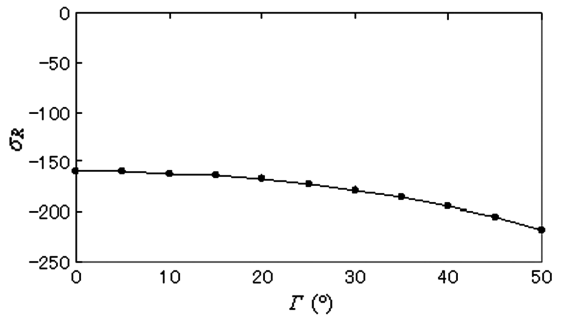

b)

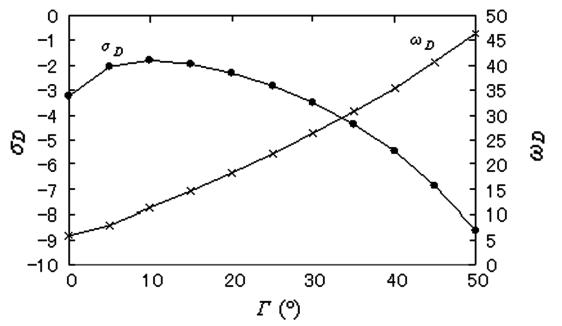

c)

Fig. 4 Eigenvalues for three modes of lateral-directional motion: a) spiral, b) roll, and c) Dutch roll.

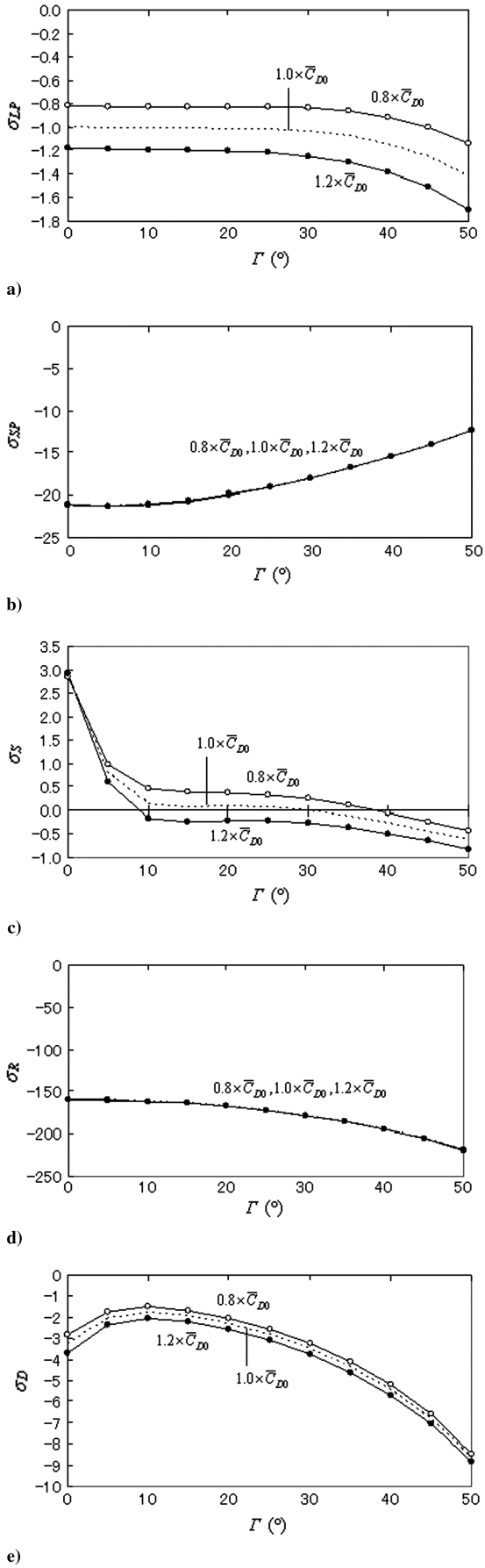

Fig. 5 Effects of C_{D0} on real parts of eigenvalues: a) long-period mode, b) short-period mode, c) spiral mode, d) roll mode, and e) Dutch roll mode.

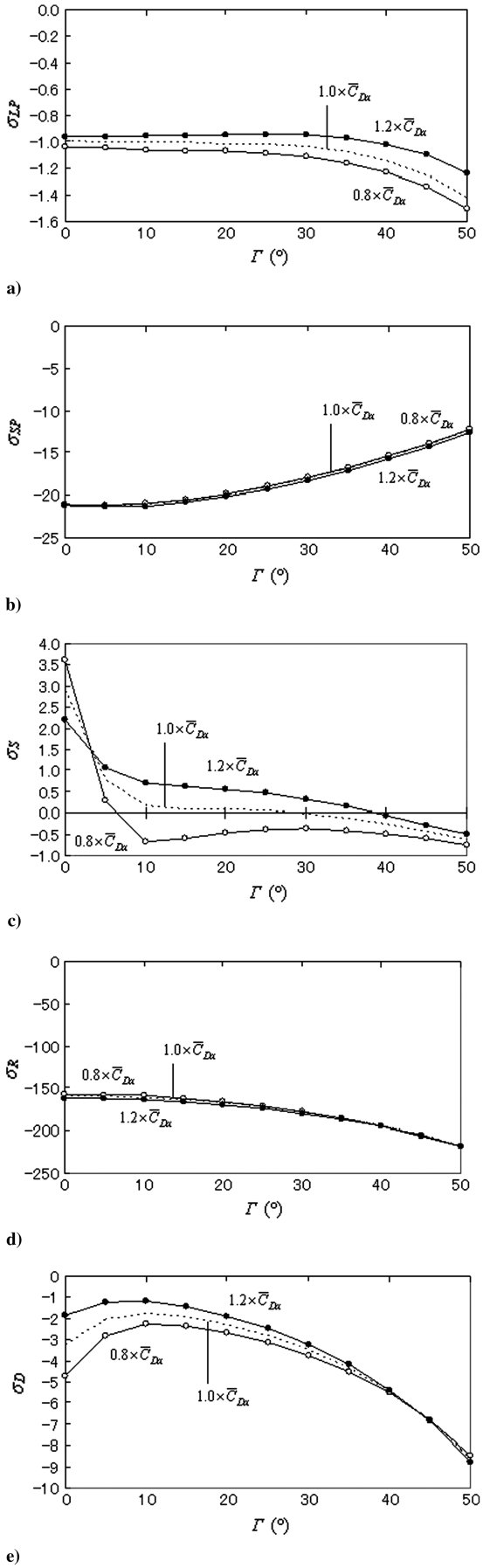

Fig. 6 Effects of $C_{D\alpha}$ on real parts of eigenvalues: a) long-period mode, b) short-period mode, c) spiral mode, d) roll mode, and e) Dutch roll mode.

be measured in a wind-tunnel test for which the results will be given next. The $\partial C_L/\partial \beta_W$ is given by

$$\frac{\partial C_L}{\partial \beta_W} = \left(2C_{L0} + \frac{\partial C_L}{\partial \alpha_W}\alpha_W\right)\tan(\Lambda + \alpha_0 \sin\Gamma) \tag{12}$$

where

$$C_L = C_{L0} + \frac{\partial C_L}{\partial \alpha_W}\alpha_W = C_{L0,\Lambda=0}\cos^2(\Lambda - \beta_W) + \left(\frac{\partial C_{L0}}{\partial \alpha_W}\right)_{\Lambda=0}\cos(\Lambda - \beta_W)\alpha_W$$

and $\beta_W = -\alpha_0 \sin\Gamma$.

Results and Discussion

Figure 3 shows the results of the longitudinal motion: the eigenvalues of A_1. Matrix A_1 has four eigenvalues; two conjugate complex numbers:

$$\begin{bmatrix} X_u & X_\alpha & X_q & -g\cos\theta_0 \\ \frac{Z_u}{U_0} & \frac{Z_\alpha}{U_0} & 1+\frac{Z_q}{U_0} & -\frac{g\sin\theta_0}{U_0} \\ M_u & M_\alpha & M_q & 0 \\ 0 & 0 & 1 & 0 \end{bmatrix}$$

Figures 3a and 3b show eigenvalues $\lambda = \sigma \pm i\omega$ of the long- and short-period modes, respectively. Since the value of σ for both modes is negative for any Γ, these modes are stable for any Γ. When $\Gamma < 30°$, the σ_{LP} of the long-period mode is independent of Γ. However, when $\Gamma > 30°$, σ_{LP} decreases with an increase of Γ. Then the long-period mode becomes more stable with an increase of $\Gamma(>30°)$. The σ_{SP} of the short-period mode increases with an increase of Γ, and the short-period mode becomes more unstable with an increase of Γ. The comparison of $|\sigma|$ between both modes shows that the $|\sigma|$ of the short-period mode is larger than that of the long-period mode. Therefore, the motion of the short-period mode converges quicker than that of the long-period mode.

Figure 4 shows the results of the lateral-directional motion: the eigenvalues of A_2. Matrix A_2 has four eigenvalues; two real numbers and one conjugate complex number:

$$\begin{bmatrix} \frac{Y_\beta}{U_0} & \frac{Y_r}{U_0}-1 & \frac{g\cos\theta_0}{U_0} & \frac{Y_p}{U_0} \\ N'_\beta & N'_r & 0 & N'_p \\ 0 & \tan\theta_0 & 0 & 1 \\ L'_\beta & L'_r & 0 & L'_p \end{bmatrix}$$

The two real eigenvalues are for the spiral and roll modes, and the one conjugate complex eigenvalue is for the Dutch roll mode. Figures 4a–4c show σ for the spiral, roll, and Dutch roll modes, respectively. Figure 4a shows that σ_S decreases with an increase of Γ and that the value is negative when $\Gamma > 30°$. Then the spiral mode becomes more stable, and its motion is stable when $\Gamma > 30°$. Moreover, σ_S is strongly affected by the variation of Γ when $\Gamma < 10°$. This feature is well known for a meter-sized airplane with vertical and horizontal tails. Note that its dihedral angle is less than 10°. Figure 4b shows that σ_R is negative for any Γ and that it decreases with an increase of Γ. Then the roll mode is stable for any Γ and becomes more stable with an increase of Γ. The $|\sigma_R|$ is very large, and the motion of the roll mode quickly converges. The variation of Γ does not strongly affect σ_R when $\Gamma < 10°$. This feature is well known for a meter-sized airplane with vertical and horizontal tails. Figure 4c shows that σ_D is negative for any Γ, and the motion of the Dutch roll mode is stable for any Γ. With an increase of Γ, σ_D increases when $\Gamma < 10°$. Conversely, the value decreases with an increase of Γ when $\Gamma > 10°$. When $\Gamma < 10°$, this feature can be observed for a meter-sized airplane with vertical and horizontal tails. When $\Gamma < 10°$, the feature is not the same as that observed in our previous work [1]. This discrepancy will be explained next.

As stated previously, all the longitudinal and lateral-directional motions are stable for any Γ, except for the spiral mode, which is only stable for $\Gamma > 30°$. This result for the lateral-direction motion, which is the same as that indicated in our previous analysis [1], can also be expected in the present analysis, where both the longitudinal and lateral-directional motions are considered: the large dihedral angle of the swallowtail is caused by stabilizing its motion of the spiral mode.

The approximated equations for the real part of the eigenvalues of the modes are indicated in [2,3]. The approximated equation for σ_{LP} in the long-period mode is given by [2]: $\sigma_{\mathrm{LP}} = \frac{1}{2}X_u$. As Γ increases, the value of $X_u < 0$ decreases and σ_{LP} decreases. The approximated equation for σ_{SP} in the short-period mode is given by [2]: $\sigma_{\mathrm{SP}} = (1/2)(Z_\alpha/U_0 + M_q)$. As Γ increases, the value of $Z_\alpha < 0$ increases, and $M_q < 0$ decreases. Furthermore, the increase of the former is larger than the decrease of the latter. With an increase of Γ, σ_{SP} increases . The approximated equation for σ_R in the roll mode is given by [3]: $\sigma_R = L'_p$. As Γ increases, $L'_p < 0$ decreases, and σ_R also decreases. Referring to [2], the approximated equation for σ_S in the spiral mode can be obtained by

$$\sigma_S = \frac{g\{(L'_\beta N'_r - N'_\beta L'_r)\cos\theta_0 - (L'_\beta N'_p - N'_\beta L'_p)\sin\theta_0\}}{-(L'_p N'_r - N'_p L'_r)Y'_\beta + U_0(L'_\beta N'_p - N'_\beta L'_p) - g(L'_\beta \cos\theta_0 + N'_\beta \sin\theta_0)} \tag{13}$$

When the stability derivatives in this equation are estimated by Eqs. (5–12), σ_S agrees well with the results shown in Fig. 4a. The approximated equation for σ_D in the Dutch roll mode [3] is given by

$$\sigma_D = \frac{1}{2}\left(N'_r - \frac{N'_p}{L'_p}L'_r + \frac{N'_p}{L'^2_p}L'_\beta\right) \tag{14}$$

When the stability derivatives in this equation are estimated by Eqs. (5–12), the relation between σ_D and Γ agrees qualitatively with that shown in Fig. 4c.

From the previous discussion, except for the Dutch roll mode, the approximated equations for the real part of the eigenvalues are clearly available quantitatively for the wide range of Γ when the stability derivatives are estimated using Eqs. (5–12).

The differences in flight stability between the swallowtail and a meter-sized airplane with vertical and horizontal tails are probably caused by the differences in Re and the airframe configurations, including the existences of the vertical and horizontal tails. Next, the differences only caused by Re are discussed. Laitone [4], Sunada et al. [5], and Sunada and Kawachi [6] pointed out that a_D, as well as C_{D0}, increases with a decrease of Re. In their analyses, a three-dimensional drag coefficient is expressed as $C_D \approx C_{D0} + a_D(\alpha\cos\Gamma)^2$. The present analysis made a stability analysis by varying the values of C_{D0} and $C_{D\alpha} = \partial C_D/\partial\alpha_W$. Note that both $C_{D\alpha}$ and a_D indicate a rate of the increase of C_D with that of α. In Figs. 5 and 6, which show the real part of eigenvalue σ of all the modes, $C_{D0} = 0.8 \times \bar{C}_{D0}$, $1.0 \times \bar{C}_{D0}$, and $1.2 \times \bar{C}_{D0}$; and $C_{D\alpha} = 0.8 \times \bar{C}_{D\alpha}$, $1.0 \times \bar{C}_{D\alpha}$, and $1.2 \times \bar{C}_{D\alpha}$, respectively. Here, $\bar{C}_{D0}$ and $\bar{C}_{D\alpha}$ are the

values of the swallowtail. The variations of C_{D0} and $C_{D\alpha}$ do not affect σ_{SP} and σ_R. With an increase of $C_{D\alpha}$ and a decrease of C_{D0}, σ_{LP} increases. The variation of σ_{LP} due to that of $C_{D\alpha}$ increases with an increase of Γ. On the other hand, the variation of σ_{LP} due to that of C_{D0} is independent of Γ.

Figure 6c shows that σ_S decreases with an increase of $C_{D\alpha}$ when $\Gamma < 4^\circ$. Conversely, σ_S increases with an increase of $C_{D\alpha}$ when $\Gamma > 4^\circ$. With an increase of C_{D0}, σ_S decreases, except when $\Gamma \approx 0^\circ$. When $\Gamma \approx 0^\circ$, σ_S is independent of C_{D0}. Figures 5e and 6e show that σ_D decreases with an increase of C_{D0}, and σ_D increases with an increase of $C_{D\alpha}$, respectively, when $\Gamma < 40^\circ$. Conversely, σ_D decreases with an increase of $C_{D\alpha}$ when $\Gamma > 40^\circ$. The variation of σ_D due to that of $C_{D\alpha}$ is larger as Γ decreases. When Γ is small, σ_D increases with an increase of Γ. This relation, when Γ is small, is different from that obtained by our previous analysis [1], where σ_D decreases with an increase of Γ. Furthermore, this relation is the same as that for a meter-sized airplane with vertical and horizontal tails. The difference between our present and previous analyses [1] can be explained as follows. The pitching moment around the center of gravity at the trimmed flight was more strictly required to be zero in the present analysis than in our previous analysis [1]. This difference is caused by the angle of attack α_0. During the trimmed flight, $\alpha_0 = 7^\circ/\cos\Gamma$ in the present analysis, but $\alpha_0 = 10^\circ$ in our previous analysis. This difference in α_0 caused the differences of C_L, C_D, U_0, and θ_0. The differences in C_L and C_D are also partially caused by the results of the wind-tunnel tests between the two analyses. These differences caused the variation in the relation between σ_D and Γ when Γ is small.

Conclusions

The stability of the longitudinal and lateral-directional motions of swallowtail butterfly *Papilio xuthus* was analyzed. The analysis indicated that all the modes in the longitudinal and lateral-directional motions are stabilized when dihedral angle Γ is larger than 30°.

We also previously analyzed the stability of the lateral-directional motion [1]. The difference between the results of our present and previous analyses is the relation between Γ and an eigenvalue of the Dutch roll mode σ_D at small Γ. In the present analysis, σ_D increases with an increase of Γ. The relation was opposite in the previous analysis. This difference was caused by the improvement of the present analysis; the pitching moment around the center of gravity is more strictly zero in the trimmed condition. The improvement makes the trimmed pitch angle in the present analysis less than in our previous analysis.

The effects of the Reynolds number, that is, C_{D0} and $C_{D\alpha}$, on the motions of all the modes in the longitudinal and lateral-directional motions were analyzed. Both C_{D0} and $C_{D\alpha}$ increase with a decrease of Re. When C_{D0} increases, the motions of the long-period, spiral, and Dutch roll modes become more stable. Conversely, when $C_{D\alpha}$ decreases, the motions of these modes become more stable. The motions of the short-period and roll modes are independent of C_{D0} and $C_{D\alpha}$.

Acknowledgment

The present study was supported in part by the Ministry of Education, Culture, Sports, Science and Technology through a Grant-in-Aid for Scientific Research (S) (18100002).

References

[1] Okamoto, M., Sunada, S., and Tokutake, H., "Stability Analysis of Gliding Flight of a Swallowtail Butterfly *Papilio Xuthus*," *Journal of Theoretical Biology*, Vol. 257, No. 2, 2009, pp. 191–202. doi:10.1016/j.jtbi.2008.11.012

[2] MaRuer, D., Ashkenas, I., and Graham, D., *Aircraft Dynamics and Automatic control*, Princeton Univ. Press, Princeton, NJ, 1973, pp. 296–418.

[3] Seckel, E., *Stability and Control of Airplanes and Helicopters*, Academic Press, New York, 1964, pp. 260–276.

[4] Laitone, E. V., "Wind Tunnel Tests of Wings at Reynolds Numbers Below 70000," *Experiments in Fluids*, Vol. 23, No. 5, 1997, pp. 405–409. doi:10.1007/s003480050128

[5] Sunada, S., Yasuda, T., Yasuda, K., and Kawachi, K., "Comparison of Wing Characteristics at an Ultralow Reynolds Number," *Journal of Aircraft*, Vol. 39, No. 2, 2002, pp. 331–338. doi:10.2514/2.2931

[6] Sunada, S., and Kawachi, K., "Effects of Reynolds Number on Characteristics of Fixed and Rotary Wings," *Journal of Aircraft*, Vol. 41, No. 1, 2004, pp. 189–192. doi:10.2514/1.2695

E. Livne
Associate Editor